Indian Journal of Chemistry
Vol. 64, December 2025, pp. 1164-1179
DOI: 10.56042/ijc.v64i12.20216

Molecular docking, dynamics simulation, DFT, MEP, PASS and ADMET approaches to methyl α-D-glucopyranoside derivatives for potential inhibitors of chikungunya virus

Nazia Islam[a], Supriyo Saha[b] & Sarkar M A Kawsar*[a]

[a] Laboratory of Carbohydrate and Nucleoside Chemistry (LCNC), Department of Chemistry, Faculty of Science, University of Chittagong, Chittagong-4331, Bangladesh

[b] Department of Pharmaceutical Chemistry, Uttaranchal Institute of Pharmaceutical Sciences, Uttaranchal University, Dehradun 248 007, Uttarakhand, India

E-mail: akawsarabe@yahoo.com

Received 31 May 2025; accepted (revised) 4 December 2025

This study investigates the development of novel carbohydrate derivatives derived from methyl α-D-glucopyranoside and their potential applications in drug development. The derivatives of methyl α-D-glucopyranoside and the parent compound have been optimized through advanced quantum mechanical methods, and density functional theory (DFT) calculations have been carried out at the B3LYP level of theory with the 6-31G++ basis set to determine their thermodynamic parameters, such as Gibbs free energy, enthalpy, entropy, and dipole moment, which have subsequently been calculated to understand their chemical behavior. Frontier molecular orbital (FMO), density of states (DOS), vibrational frequency (FT-IR), UV–visible, and molecular electrostatic potential (MEP) analyses of the seven modified compounds have been carried out. Molecular docking has been performed against the viral protein of chikungunya virus, which has revealed the binding modes, nonbonding interactions, and binding affinities of these derivatives, shedding light on their potential antiviral activity. Compared with those of methyl α-D-glucopyranoside, all the derivatives presented increased binding affinities. A 150 ns molecular dynamics simulation has been conducted to observe the behavior of the complex structure, revealing a stable conformation and binding mode in the stimulating environment of the compounds. Pharmacological and pharmacokinetic assessments, including toxicity, metabolism, and absorption, have been conducted *via* ADMET and PASS to identify the most promising candidates for future development. ADMET analysis has revealed that the derivatives have lower toxicity and improved pharmacokinetic features over those of the parent compound. This research highlights the therapeutic potential of carbohydrate-based compounds, paving the way for the development of new carbohydrate-derived drugs as potential inhibitors of the chikungunya virus.

Keywords: Chikungunya virus, DFT, Molecular docking, Molecular dynamics (MD) simulation, Methyl α-D-glucopyranoside

Carbohydrates, one of the most important dietary components, are not only a great source of energy but also essential to cell function. Carbohydrates are classified into four types on the basis of their degree of polymerization: monosaccharides, disaccharides, oligosaccharides, and polysaccharides[1,2]. Carbohydrates have received significant research attention because of their importance in immunological responses, cell proliferation, viral and bacterial infection processes, and cell-to-cell communication[3]. Both natural and synthetic carbohydrate-based compounds are recognized for their wide variety of pharmacological properties, and many of them are therapeutically employed to treat diverse illnesses[4–6]. They are structurally diverse in terms of functional groups, ring size, and linkages. Owing to their significant optical purity, bioavailability, and low toxicity, these materials are excellent scaffolds for drug development methods[7,8]. Owing to their hydrophilic nature, monosaccharides have excellent water solubility and pharmacokinetics[9]. Recent research has revealed their medical potential in the form of carbohydrate-derived medicines[10,11]. In the last two decades, several new carbohydrate-based medications have been created, assessed, and produced[12,13]. The diverse biological functions of carbohydrates provide an outline for the discovery of carbohydrate-based drugs[14]. Glycans, a specific category of carbohydrate, have been linked to various diseases, including tumors, inflammation, and microbial infections[15,16]. Vaccines, antiviral agents, and immunotherapies have been designed by exploiting specific interactions between glycans and

lectins[17-19]. Recently, modern methods have been employed for the isolation of diverse natural compounds from plants[20] and other sources, where carbohydrates are a significant component[21]. Carbohydrate-based drugs, such as dapagliflozin, plazomicin, and azvudine, may be considered possible therapeutic agents for the treatment of diabetes, bacterial infections, and viral infections in both previously treated and untreated patients (Fig. 1).

Currently, more than 170 carbohydrate-containing drugs have achieved clinical approval worldwide[22,23]. Our research developed seven carbohydrate derivatives from a single-molecule framework, methyl α-D-glucopyranoside[24,25]. After developing these derivatives, we optimized their structures and used advanced quantum mechanical methods to investigate their thermal and electrical stability, as well as their biological features. To better understand their chemical and thermal behavior[26,27], we examined parameters such as free energy, enthalpy, entropy, heat capacity, dipole moment, energy gaps between molecular orbitals, *etc*.[28–30] We also plotted the electrostatic potential to determine the reactive regions of these compounds[31].

To determine how these compounds interact with specific proteins, we conducted molecular docking against the viral protein Chikungunya virus (PDB ID: 3N40) to understand their nonbonding interactions, binding mode, and binding affinity. This allowed us to analyze how well the derivatives bind to receptor proteins and to understand the nature of these interactions. Following docking, the complex was simulated with GROMACS to observe stability in a dynamic environment[32].

We also assessed the pharmacological and pharmacokinetic features of the derivatives, taking into account parameters such as toxicity, metabolism, and absorption by the body[33,34]. We were able to identify potential candidates for future development by studying their thermodynamic characteristics, molecular structures, and biological activities. Our research focused on creating novel molecules and evaluating their computational inhibitor properties to identify possible new carbohydrate-based drugs as a potential inhibitor of the chikungunya virus.

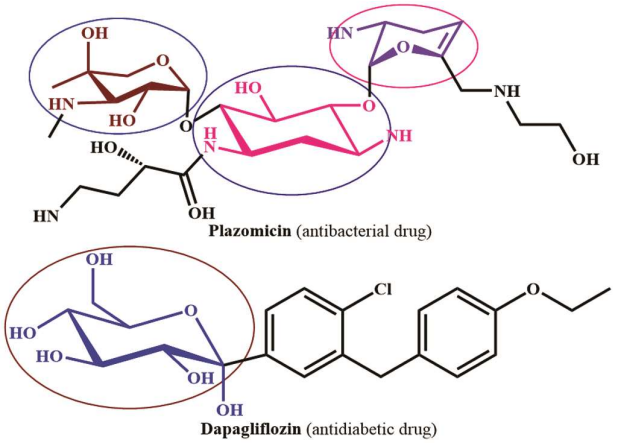

Fig. 1 — Marketed drugs having carbohydrate moieties

Experimental Details

Used Compounds

As shown in Fig. 2, we previously synthesized methyl α-D-glucopyranoside (**1**) derivatives (**2-8**) with different acylating agents in dimethyl formamide (DMF) and TEA at low temperatures[35].

We conducted the usual analysis procedure and separated the chemicals using silica gel column chromatography. The compounds' structure was ascertained with spectroscopic methods, which demonstrated the presence of a mono-substituted product.

Computational Details and Geometry Optimization

The application of computational techniques in the realms of drug discovery and development has increased greatly, as these technologies enable researchers to accurately forecast novel compounds that have yet to be recognized[36]. Rather than relying on expensive experimental trials, it is now possible to predict characteristics related to thermodynamic, geometrical, spectroscopic, molecular orbital, and biological properties through computational methods. The chemical structures of methyl α-D-glucopyranoside and its derivatives were created by ChemDraw Professional 16.0. The 2D structures were subsequently converted into 3D models incorporating hydrogen atoms in Discovery Studio Visualizer v20.1.0. Gaussian 09 W (Revision D.01) software was used for all quantum chemistry calculations, and time-dependent DFT (TD-DFT) and density functional theory (DFT) were applied at the B3LYP functional and 6-31G++ levels of theory[37] (Fig. 1S). The calculations for the HOMO-LUMO gap, hardness (η), softness (S), chemical potential (μ), electronegativity (χ), and electrophilicity (ω) were performed *via* the specified formulas[38].

$$\text{Gap } (\Delta E) = [\varepsilon LUMO - \varepsilon HOMO]$$

$$\eta = \frac{[\varepsilon LUMO - \varepsilon HOMO]}{2}$$

$$S=\frac{1}{2\eta}$$

$$\mu=\frac{[\varepsilon LUMO + \varepsilon HOMO]}{2}$$

$$\chi = -\frac{[\varepsilon LUMO + \varepsilon HOMO]}{2}$$

$$\omega=\frac{\mu^2}{2\eta}$$

Protein Design and Molecular Docking

The crystal structure of the immature envelope glycoprotein complex of the Chikungunya virus (PDB ID: 3N40) was retrieved in pdb format from the RCSB protein data bank (https://www.rcsb.org/)[39]. The Discovery Studio Visualizer v20.1.0 program eliminates cocrystallized ligands, water molecules, unexpected chains, and heteroatoms. Swiss PDB viewer program Version 4.1.0) performed energy minimization and bad atom interaction[40]. Finally, PyRx software (version 0.8) has been utilized to perform molecular docking, taking into account the protein as a macromolecule and the chemical as a ligand[41]. The grid box sizes of AutoDock Vina were 90.408, 92.448, and 60.109 Å along the X, Y, and Z directions, respectively. To calculate and visualize nonbonding interactions, Discovery Studio Visualizer v20.1.0 was used.

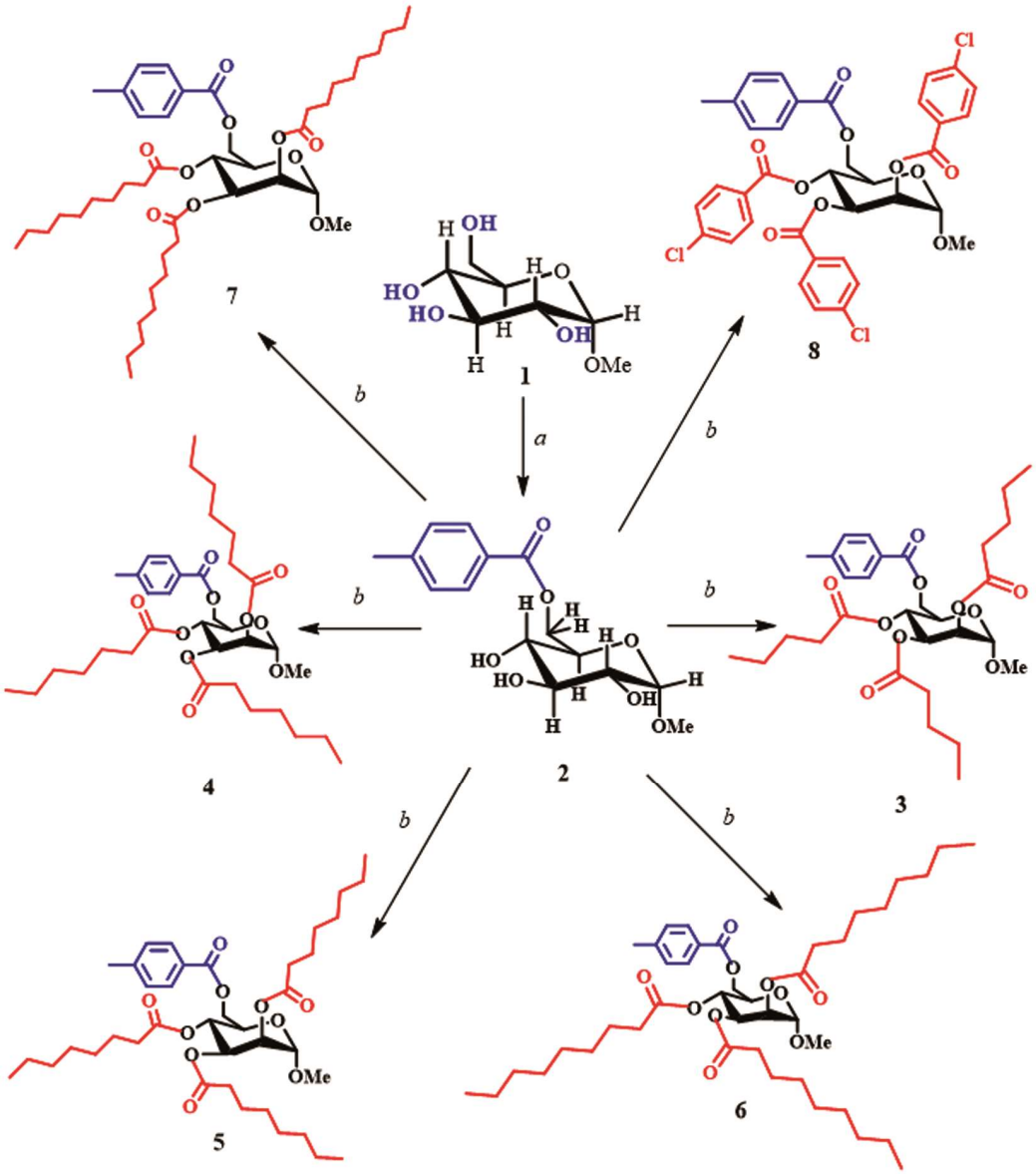

Fig. 2— Synthesized glucopyranoside derivatives (**2-8**)[35]

Molecular Dynamics Simulation

The top-ranked docked complex was selected based on binding affinity and visual inspection of interactions. This complex was subsequently used as the initial structure for molecular dynamics simulations. The docked complex was prepared for simulation using GROMACS 2023.3 package, employing the CHARMM27 force field[42]. Ligand topology was generated using SwissParam (http://swissparam.ch/) server[43], and the system was solvated in an octahedron box of TIP3P water model[44] with periodic boundary conditions. Appropriate counterions were added to neutralize the system before energy minimization and equilibration. The equilibrated protein–ligand complex was subjected to a production molecular dynamics (MD) simulation for a total duration of 150 ns (75,000,000 steps) under isothermal–isobaric (NPT) conditions. Temperature was maintained at 300 K and pressure was controlled at 1 bar.

ADMET

The admetSAR server (http://lmmd.ecust.edu.cn/admetsar1/predict/) was used to study the pharmacokinetic parameters and toxicity of the modified methyl α-D-glucopyranoside derivatives and parent compounds[45]. AdmetSAR employs structure similarity search methods to predict the latest and most extensive, manually curated data for a wide range of chemicals, linked to their known absorption, distribution, metabolism, excretion, and toxicity (ADMET) profiles. In general, drug likeness is assessed *via* Lipinski's rule of five[46]. A simplified molecular input line entry system (SMILES) was generated using the online server (https://cactus.nci.nih.gov/translate/) as input for ADMET. Drug discovery and chemical safety rely heavily on absorption, distribution, metabolism, excretion, and toxicity (ADMET) characteristics[47].

PASS Prediction

To predict drug-like chemical molecules with biological activity profiles, the PASS (prediction of activity spectra for substances) online program (http://www.way2drug.com/passonline/) based on the compound's structural formula was used[48]. The PASS program provides data on the biological activity of substances on the basis of their chemical structure[49]The current version of the PASS can predict more than 4000 biological activities. It has an accuracy of 95%[50]. A simplified molecular input line entry system (SMILES) was generated using the online server (https://cactus.nci.nih.gov/translate/) as input. It predicts the activity in terms of probability: probable activity (pa) and probable inactivity (pi). The values fall between 0.000 and 1.000[51]. The activity of a chemical compound is considered only if the pa value is greater than the pi value. Compounds with a pa value above 0.7 are thought to have superior pharmacological activity. Similarly, the likelihood of witnessing the activity is lower for compounds with a value less than 0.7[48].

Results and Discussion

Thermodynamic Analysis

The free energy and enthalpy values can be used to calculate the spontaneity of a reaction and the stability of a product. The free energy (G) is an important criterion for representing the interaction of binding partners; a negative value indicates that spontaneous binding and interaction are preferable. The ideal structures' free energy and enthalpy values are negative, implying that they are all exothermic, spontaneously react, and give reasonably stable products[52]. The dipole moment governs hydrogen bond formation and nonbonded interactions in drug design[53]. Derivative **8** has the best free energy and enthalpy values among those of the other derivatives in the presence of extra electronegative atoms (Cl), with values of –3542.3 Hartree and –3542.2 Hartree, respectively. Its dipole moment is also significantly greater (5.4484 Debye) than that of the parent compound methyl α-D-glucopyranoside (3.5085 Debye). Table 1 lists the stoichiometry, molecular weight (g/mol), electronic energy (Hartree), enthalpy (Hartree), Gibbs free energy (Hartree), and dipole moment (Debye) of the derivatives of the methyl α-D-glucopyranosides.

Frontier Molecular Orbitals (FMO)

The frontier molecular orbitals of a molecule are utilized for determining chemical reactivity and kinetic stability. The frontier molecular orbitals are the highest occupied (HOMO) and lowest unoccupied (LUMO) orbitals. Electronic absorption is the transition from the ground state to the first excited state, and it is primarily defined by single-electron excitation from the HOMO to the LUMO. Compound **8** has the lowest energy gap (4.2915 eV), suggesting that it is a more reactive and polarizable molecule due to the ease of electron transfer, with a maximum

Table 1 — Stoichiometry, molecular weight (g/mol), electronic energy (Hartree), enthalpy (Hartree), Gibbs free energy (Hartree), and dipole moment (Debye) of all the compounds

Entry	Stoichiometry	Molecular Weight (g/mol)	Electronic Energy (Hartree)	Enthalpy (Hartree)	Gibb's free Energy (Hartree)	Dipole moment (Debye)
1	$C_7H_{14}O_6$	194.08	–722.01	–722.01	–722.06	3.5085
2	$C_{15}H_{20}O_7$	312.12	–1103.7	–1103.7	–1103.8	3.1613
3	$C_{30}H_{44}O_{10}$	564.29	–1910.7	–1910.7	–1910.8	5.8839
4	$C_{36}H_{56}O_{10}$	648.39	–2145.1	–2145.1	–2145.2	4.4203
5	$C_{39}H_{62}O_{10}$	690.43	–2262.3	–2262.3	–2262.5	2.8756
6	$C_{42}H_{68}O_{10}$	732.48	–2379.5	–2379.5	–2379.7	6.2440
7	$C_{45}H_{74}O_{10}$	774.53	–2496.7	–2496.7	–2496.9	5.5294
8	$C_{37}H_{31}C_{l3}O_{10}$	740.09	–3542.2	–3542.2	–3542.3	5.4484

Table 2 — Energy (eV) of the HOMOs, LUMOs, gap, hardness (η), softness (S), chemical potential (μ), electronegativity (χ), and electrophilicity (ω) of all the compounds

Entry	ϵHOMO	ϵLUMO	Gap (Δ)	η	S	μ	χ	ω
1	–5.7947	–0.30477	5.4899	2.744965	0.182152	–3.04974	3.049735	1.69417161
2	–6.5291	–0.8656	5.6635	2.83175	0.176569	–3.69735	3.69735	2.41377188
3	–6.5528	–1.2879	5.2649	2.63245	0.189937	–3.92035	3.92035	2.91917114
4	–6.5435	–0.7823	5.7612	2.8806	0.173575	–3.6629	3.6629	2.3288267
5	–6.7201	–0.9445	5.7756	2.8878	0.173142	–3.8323	3.8323	2.54285672
6	–6.5307	–1.2734	5.2573	2.62865	0.190212	–3.90205	3.90205	2.89616233
7	–6.8194	–1.1614	5.658	2.829	0.176741	–3.9904	3.9904	2.81429695
8	–6.4632	–2.1717	4.2915	2.14575	0.233019	–4.31745	4.31745	4.34355692

softness (0.233019 eV) and chemical potential (–4.31745 eV)[54]. Compound **6** has the second-lowest energy gap (5.2573 eV) with the second-highest softness (0.190212 eV). Table 2 shows the HOMO and LUMO energies, HOMO–LUMO gap (Δ), hardness (η), softness (S), chemical potential (μ), electronegativity (χ), and electrophilicity (ω) indices for all the derivatives. The number of available electronic states at various energy levels within a compound is represented graphically by a density of states (DOS) plot. It offers information about chemical reactivity and electronic structure. The electron energy levels are shown on the X-axis. The y-axis displays the number of electronic states that are available at every energy level. While the virtual orbitals (red) possess positive energy values, the occupied orbitals (green) extend far into the negative energy region. Fig. 2S provides a clearer grasp of the HOMO–LUMO energy and energy gap. Fig. 3S shows the density of states (DOS) of the derivatives of methyl α-D-glucopyranoside.

MEP (Molecular Electrostatic Potential)

The molecular electrostatic potential (MEP) is extensively used as a reactivity map that indicates the optimal position for charged point-like reagents and electrophilic and nucleophilic attacks on organic compounds[55]. This study contributes to our understanding of the biological recognition process and hydrogen bonding interactions[56]. MEP is important for color grading since it shows the molecule size, shape, and positive, negative, and neutral electrostatic potential zones. Potential increases are listed in the following order: red, orange, yellow, green, and blue. The largest negative region is shown in red, suggesting a suitable location for electrophilic attack. The blue tint denotes the most positive area suited for nucleophilic attack. The color green represents zero potential zones. Table 3 shows the molecular electrostatic potential of the derivatives of methyl α-D-glucopyranoside.

Vibrational Frequency (FT-IR)

Infrared (IR) spectroscopy provides vital information on molecular vibrations, which aids in the identification of functional groups. To illustrate the presence of vibrational frequencies between 400 and 4000 cm^{-1}, they are computed *via* computational methods[57,58]. The accuracy level was enhanced by multiplying the estimated frequencies by a scaling factor (0.9688)[59]. Compounds **1-8** exhibit vibrational frequencies such as C-H stretching (C-Ha, C-H), carbonyl stretching (C=O), and O-H stretching. The frequency range for C–Ha stretching is 2983–3250 cm^{-1}, C–H stretching is 3022–3205 cm^{-1}, C=O (carbonyl stretching) is 1710–1788 cm^{-1}, and -OH

Table 3 — Molecular electrostatic potential of the derivatives of methyl α-D-glucopyranoside

Entry	
	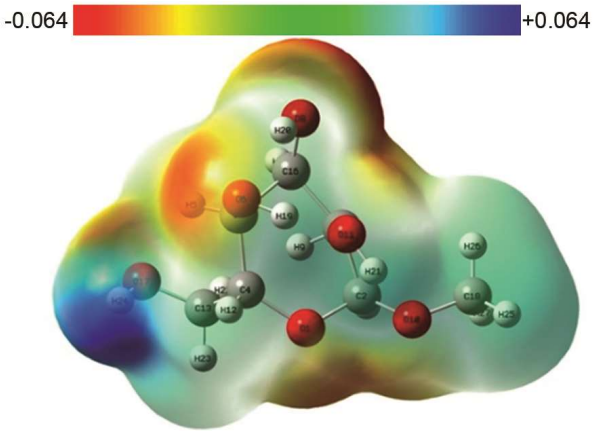
	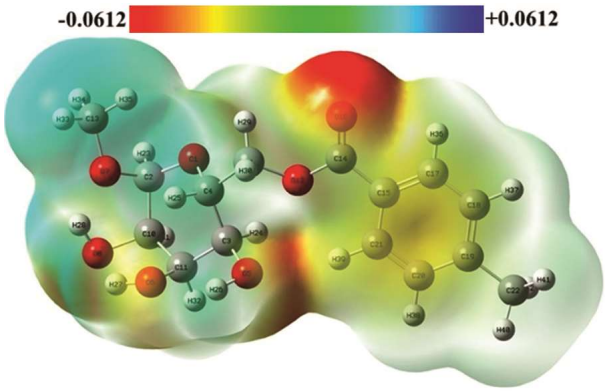
	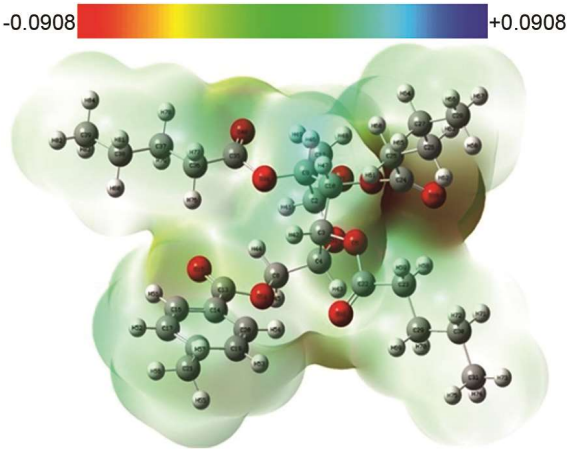
	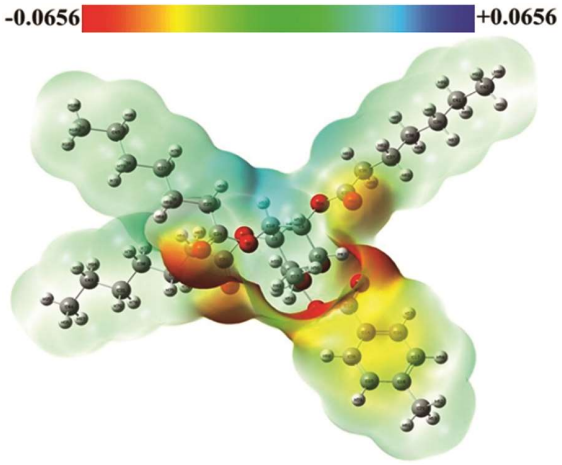
	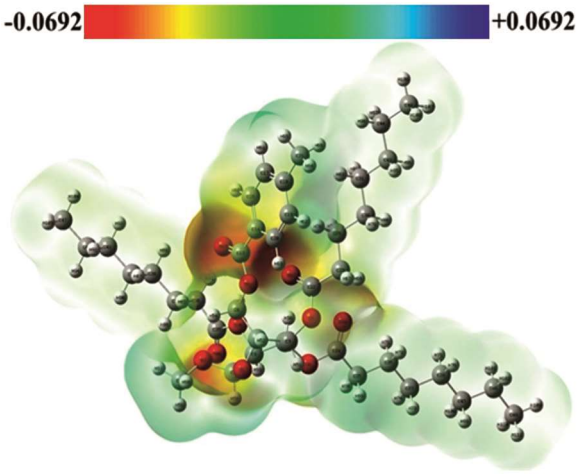
	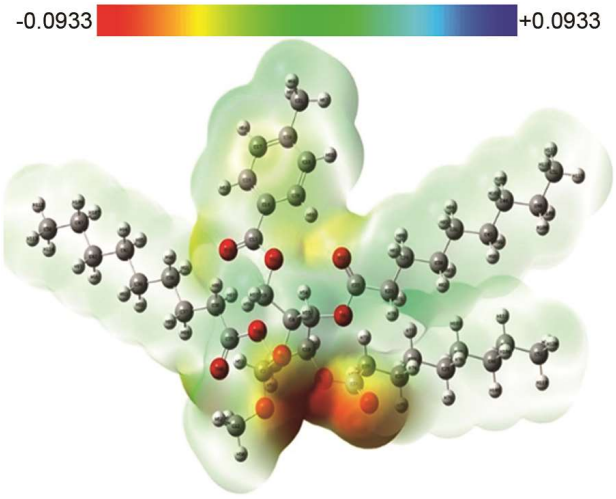

(*Contd*.)

Table 3 — Molecular electrostatic potential of the derivatives of methyl α-D-glucopyranoside (*Contd*.)

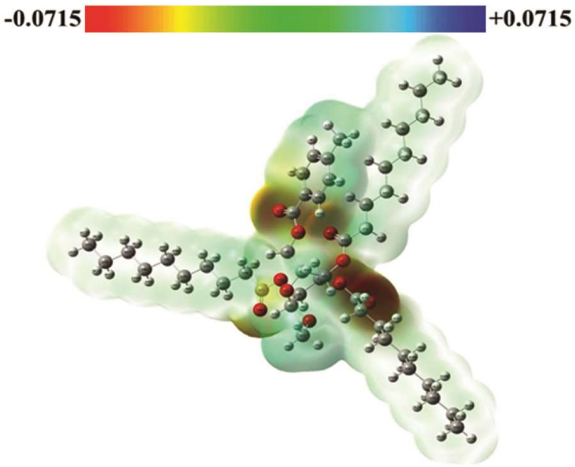

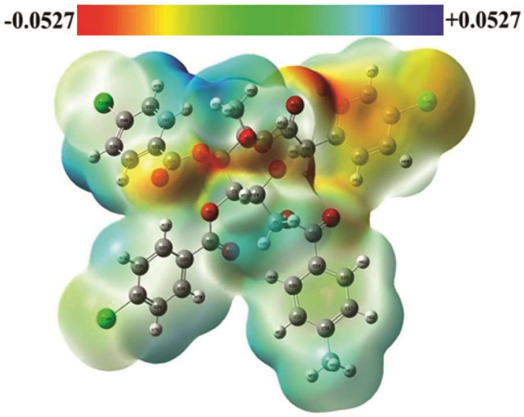

(hydroxyl stretching) is 3200–3467 cm^{-1}. OH stretching is only observed in compounds **1** and **2**. This indicates the presence of an -OH group. Compounds **2-8** exhibit stretching of C-Ha, C-H, and C=O. In Table 4, several major vibrational frequencies are shown, and Fig. 3 displays the overall infrared spectrum.

UV-Visible Absorption

UV–visible absorption spectra are generated by electronic transitions in molecules, especially those that occur between ground-state and excited-state molecular orbitals (MOs)[60]. Table 5 shows the electrical transition stages of the analogs from the ground state (S0) to the singlet state (S1). Methyl α-D-glucopyranoside derivatives **2-8** absorb in a shorter wavelength range (236.75–309.29 nm) and have oscillator strengths ranging from 0.0001-0.0122. At 309.29 nm, derivative **8** has the highest wavelength at an oscillator strength of 0.0001. The derivative **8**'s maximum wavelength is defined by charge transfer from the excited state S0 to S1, which is H-1 →L (0.10074), H →L (0.69382). It has the lowest excitation energy (4.0086 eV) and is more reactive than methyl α-D-glucopyranoside (Fig. 4).

Molecular Docking and Interactions Calculations

Molecular docking is a computational approach for predicting the binding relationship between a ligand and a target protein. It aids in drug development by simulating how small molecules interact with biological targets to inhibit or stimulate activities[61,62]. Molecular docking was performed *via* Autodock Vina for compounds **1** to **8** into the viral protein

Table 4 — Selected vibration frequencies of the derivatives of methyl α-D-glucopyranoside

Entry	Assignment	Vibrational Frequency (cm^{-1})
1	vC-H[a]	–
	vC-H	3038-3168
	vC=O	–
	vO-H	3200-3467
2	vC-H[a]	3189-3218
	vC-H	3028-3173
	vC=O	1745
	vO-H	3251-3411
3	vC-H[a]	2983-3228
	vC-H	3078.33-3205
	vC=O	1719-1783
	vO-H	–
4	vC-H[a]	3201-3250
	vC-H	3025-3150
	vC=O	1744-1 788
	vO-H	–
5	vC-H[a]	3190-3242
	vC-H	3025-3160
	vC=O	1742-1781
	vO-H	–
6	vC-H[a]	3191-3239
	vC-H	3023-3166
	vC=O	1710-1794
	vO-H	–
7	vC-H[a]	3192-3241
	vC-H	3022-3162
	vC=O	1744-1773
	vO-H	–
8	vC-H[a]	3193-3246
	vC-H	3023-3188
	vC=O	1713-1769
	vO-H	–

Chikungunya virus (CHIKV) PDB ID: 3N40. Compared with the parent compound methyl α-D-glucopyranoside (–4.7 kcal/mol), all the compounds

Table 5 — Electronic absorption of methyl α-D-glucopyranoside (**1**) and its derivatives (**2-8**)

Entry	Excited State	Wavelength (nm)	Excitation Energy (eV)	Configuration Composition	Oscillator Strength
1	$S_0 \rightarrow S_1$	263.91	4.6979	L-1 →H (-0.13867) H →L (0.68581)	0.0074
2	$S_0 \rightarrow S_1$	263.36	4.7078	H-4 → L (-0.28549) H-3→L (0.56221) H-3→L+3 (0.10720) H-1 →L (-0.27590)	0.0066
3	$S_0 \rightarrow S_1$	259.79	4.7725	H-6→L (0.28175) H-5 →L (0.22005) H-4 →L (-0.13055) H →L (0.58454)	0.0027
4	$S_0 \rightarrow S_1$	259.14	4.7845	H-4→L (-0.20086) H-3→L (0.65787) H-3→L+6 (-0.10530)	0.0008
5	$S_0 \rightarrow S_1$	265.63	4.6675	H-5 →L (0.11755) H-2 →L (0.30923) H-1 →L (0.59223) H →L (-0.10259)	0.0013
6	$S_0 \rightarrow S_1$	259.98	4.7691	H-7 →L (-0.18187) H-5 →L (0.31690) H-4 →L (-0.13120) H →L (0.58101)	0.0013
7	$S_0 \rightarrow S_1$	236.75	5.2369	H-4 →L (-0.13084) H-3→L (0.65620) H-1 →L (-0.12553)	0.0122
8	$S_0 \rightarrow S_1$	309.29	4.0086	H-1 →L (0.10074) H →L (0.69382)	0.0001

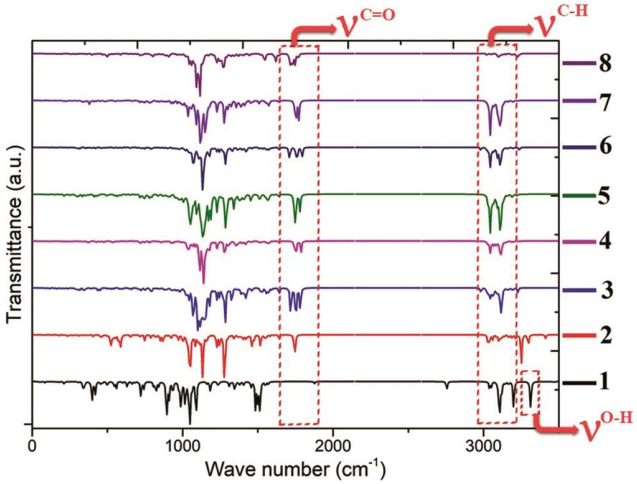

Fig. 3 — The overall infrared spectra of methyl α-D-glucopyranoside and its derivatives

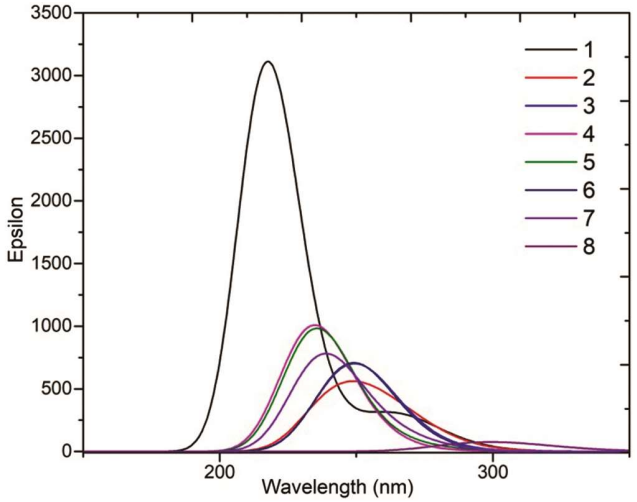

Fig. 4 — UV–visible spectra of methyl α-D-glucopyranoside and its derivatives

(**2-8**) presented increased binding affinity, ranging from –6.0 kcal/mol to –8.8 kcal/mol. Compound **2** and **8** have the highest binding affinities for the 3N40 protein, measuring –8.8 and –6.9 kcal/mol, respectively. The docking score of compound **3**, however, is fairly high at –6.8 kcal/mol, with significant number of alkyl and pi-alkyl interactions. However, Derivatives **5** and **6** have the same binding affinity of –6.2 kcal/mol, with similar residues in contact and interaction types. All of the investigated compounds bound to the appropriate binding pocket in the receptor protein and hit the majority of the targeted amino acid residues. Table 6 shows the binding affinity and nonbonding interactions of methyl α-D-glucopyranoside and its derivatives with the receptor protein 3N40, and in Fig. 5, the binding

Table 6 — Binding affinity and nonbonding interactions of methyl α-D-glucopyranoside and its derivatives with the receptor protein 3N40

Entry	Binding affinity (kcal/mol)	Residue in contact	Interaction type	Bond distance (Å)
1	–4.7	THR384	H	2.06923
		ASN363	H	2.85876
		ASN363	H	2.243
		ASN369	H	2.45648
		ASN369	H	2.3232
		THR38	H	2.0047
2	–6.9	PRO198	H	2.71962
		ARG168	H	1.98297
		ILE200	H	2.529
		PHE205	H	2.74338
		VAL199	C	3.38984
		LYS204	PC	4.99151
		LYS204	A	4.92066
		VAL199	PA	5.11001
		LYS204	PA	3.64005
3	–6.8	ARG168	H	2.92174
		PHE205	H	2.28828
		PRO197	C	3.45642
		LYS204	PS	3.54123
		LYS204	A	5.10971
		PRO356	A	4.17364
		ILE200	A	4.02227
		LYS171	A	5.1615
		PRO197	A	5.36574
		ARG208	A	3.70515
		CYS330	A	4.99034
		PRO356	PA	5.49142
		PHE205	PA	5.07313
		HIS206	PA	4.26213
4	–6.0	ARG168	H	2.16781
		ARG168	H	2.96597
		THR106	C	3.65478
		PRO198	C	3.10447
		HIS206	C	3.47917
		ARG208	A	4.30901
		CYS330	A	3.87025
		LYS204	A	4.2725
		CYS330	A	4.06763
		PRO356	A	5.29374
		LYS171	PA	4.58483
5	–6.2	ARG168	H	2.16781
		ARG168	H	2.96597
		THR106	C	3.65478
		PRO198	C	3.10447
		HIS206	C	3.47917
		ARG208	A	4.30901
		CYS330	A	3.87025
		LYS204	A	4.2725
		CYS330	A	4.06763
		PRO356	A	5.29374
		LYS171	PA	4.58483

(*Contd*.)

Table 6 — Binding affinity and nonbonding interactions of methyl α-D-glucopyranoside and its derivatives with the receptor protein 3N40 (*Contd*.)

Entry	Binding affinity (kcal/mol)	Residue in contact	Interaction type	Bond distance (Å)
6	–6.2	ARG168	H	2.16781
		ARG168	H	2.96597
		THR106	C	3.65478
		PRO198	C	3.10447
		HIS206	C	3.47917
		ARG208	A	4.30901
		CYS330	A	3.87025
		LYS204	A	4.2725
		CYS330	A	4.06763
		PRO356	A	5.29374
		LYS171	PA	4.58483
7	–6.4	ARG168	H	2.16781
		ARG168	H	2.96597
		THR106	C	3.65478
		PRO198	C	3.10447
		HIS206	C	3.47917
		ARG208	A	4.30901
		CYS330	A	3.87025
		LYS204	A	4.2725
		CYS330	A	4.06763
		PRO356	A	5.29374
		LYS171	PA	4.58483
8	–8.8	ARG168	H	2.16781
		ARG168	H	2.96597
		THR106	C	3.65478
		PRO198	C	3.10447
		HIS206	C	3.47917
		ARG208	A	4.30901
		CYS330	A	3.87025
		LYS204	A	4.2725
		CYS330	A	4.06763
		PRO356	A	5.29374
		LYS171	PA	4.58483

H = Conventional hydrogen bond, C = Carbon hydrogen bond, A = Alkyl, PA = Pi-alkyl, PS = Pi-sigma, PC = Pi-Cation, Psu = Pi-Sulfur, PPTSh = Pi-Pi T-shaped, PPS = Pi-Pi stacked

pockets, binding interactions, and hydrogen bonds of derivatives **2**, **3** and **8** have the highest binding affinities of –6.9, –6.8 and –8.8 kcal/mol, respectively.

Molecular Dynamics Simulation Study

The results of the molecular docking analysis revealed that protein–ligand complexes **2** (PL2) and **8** (PL8) have the highest binding affinities, which are –6.9 kcal/mol and –8.8 kcal/mol, respectively. To establish their binding affinities, deviations, and shifts from the binding pockets, a molecular dynamics simulation was performed. Fig. 6 shows the RMSD (root mean square deviation) profiles of compounds **2** (represented in red) and **8** (represented in blue) over a 150 ns molecular dynamics simulation. The RMSD was calculated with respect to the initial minimized structure *via* GROMACS. The X-axis representsthe simulation time from 0 to 150 ns. The Y-axis represents the RMSD in nm, which is the average deviation of the atomic positions from the starting structure. For compound **2** (red curve) at the initial phase (0–90 ns)**,** the RMSD remains relatively stable between 0.3–0.6 nm with some fluctuations, suggesting structural stability during this period. During the middle to late simulations (90–135 ns), the RMSD sharply increased, with spikes reaching ~2.0 nm at 110 ns and approximately at 135 ns. This suggests significant structural rearrangements or flexibility during this period. At the end of the phase (135–150 ns), it stabilizes again at ~0.5 nm, indicating that the structure may have settled into a new

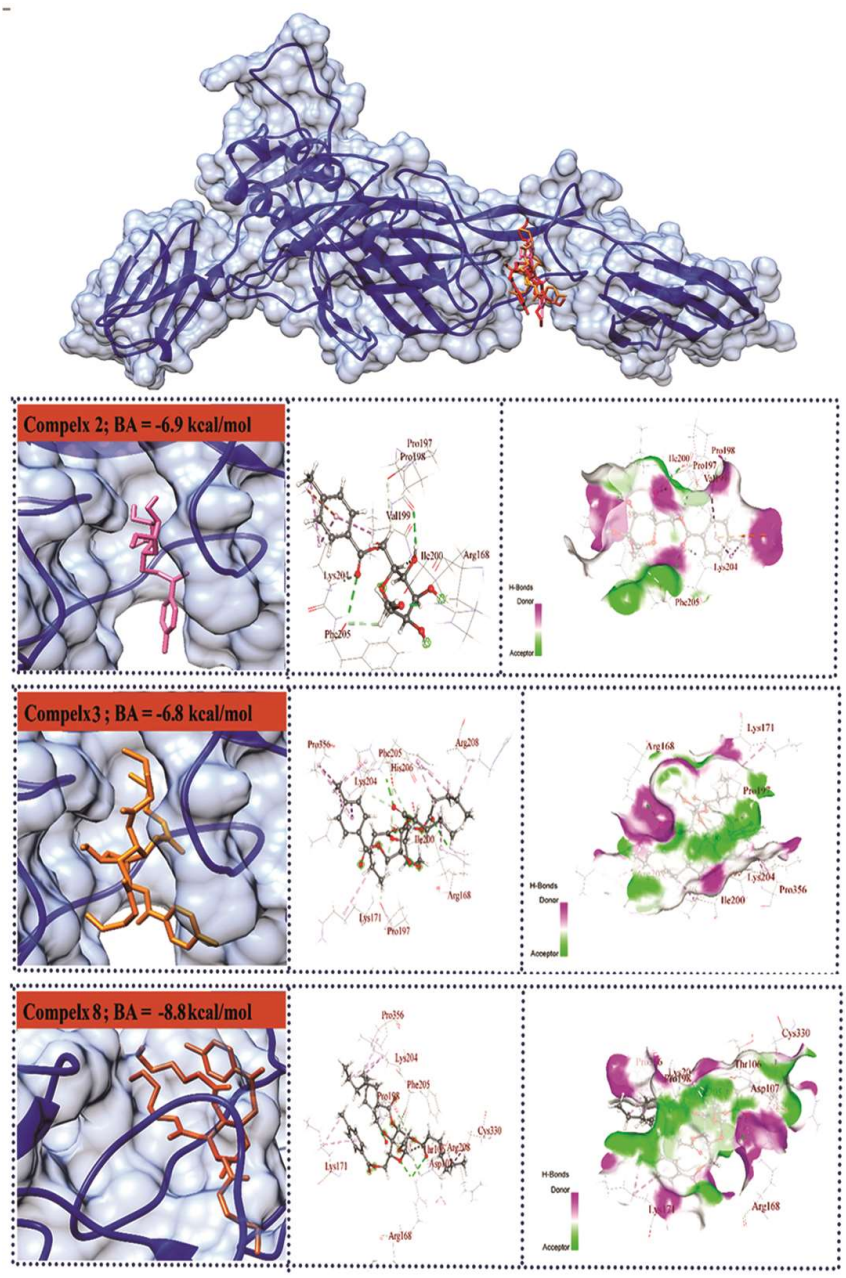

Fig. 5 — The protein–ligand complex, binding pockets, nonbinding interactions and hydrogen bonds of derivatives **2**, **3** and **8** with the receptor protein 3N40

conformation. However, for compound **8** (blue curve) during the entire simulation (0–150 ns), the RMSD remained consistent at approximately 0.4–0.6 nm, with minor fluctuations. No major spikes or structural deviations were observed. These findings suggest that compound **8** is structurally more stable throughout the simulation. Compared with compound **8**, compound **2** appears to be less stable and undergoes large conformational changes during the simulation. A possible unfolding or major rearrangement occurred.

The root mean square fluctuation (RMSF) plot provides insights into the flexibility of individual protein residues during molecular dynamics (MD) simulation. The structural effects of compound **2** (represented in red) and compound **8** (represented in blue) in RMSF quantify the average positional deviation of each residue over time, highlighting regions of structural rigidity and flexibility. Both compounds exhibit a characteristic pattern of alternating peaks and troughs across the residue

index, corresponding to flexible loops and rigid secondary structure elements. However, notable differences emerge in the amplitude and distribution of these fluctuations between compounds **2** and **8**. Fig. 7 shows the RMSF graphs of compounds **2** and **8**. Compound **8** generally induced lower fluctuations, suggesting that it stabilized the protein structure more effectively. It shows a significant RMSF spike around residue 60, peaking at approximately 0.65 nm, which may correspond to a loop or unstructured domain that is inherently flexible. Outside of this region, compound **8** maintains relatively modest fluctuations at approximately 0.1–0.3 nm, indicating consistent structural stability across most of the protein. In contrast, compound **2** has higher RMSF values in several key regions, particularly between residues 250–400, with peaks approaching 0.5–0.6 nm. This finding suggests increased flexibility or partial destabilization in these segments, possibly affecting the protein's functional or binding regions. Additionally, the RMSF values for compound **2** remain consistently greater than those for compound **8** across many residues, implying that compound **2** may induce localized conformational changes or less stable interactions with the protein. These findings align with prior RMSD analysis, where compound **8** maintained a more stable overall conformation, whereas compound **2** displayed significant global fluctuations during the simulation. Together, the RMSF and RMSD results suggest that compound **8** is the more structurally stabilizing ligand, whereas compound **2** promotes greater conformational flexibility, which may impact binding affinity or functional modulation.

The solvent accessible surface area (SASA) is a key parameter used to assess the extent to which a protein's surface is accessible to solvent molecules during an MD simulation. Changes in SASA reflect conformational shifts, such as folding, unfolding, or ligand-induced compaction of the protein structure. A lower SASA value generally indicates a more compact and less solvent-exposed protein conformation, whereas a higher SASA implies a more open or flexible structure. The SASA profiles of the protein–ligand complexes with compound **2** and compound **8** were monitored over 150 ns, providing insight into the stability and compactness of the complexes. Fig. 8 represents the solvent accessible surface area (SASA) over time (ns) for two molecular systems: "PL2–3N40" (red line) and "PL8–3N40" (blue line). The SASA values for the protein

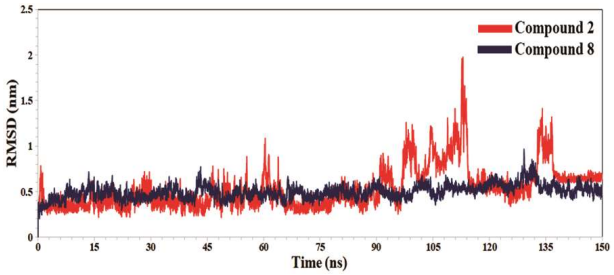

Fig. 6 — Time-dependent RMSD profiles of compounds **2** and **8** during molecular dynamics simulation

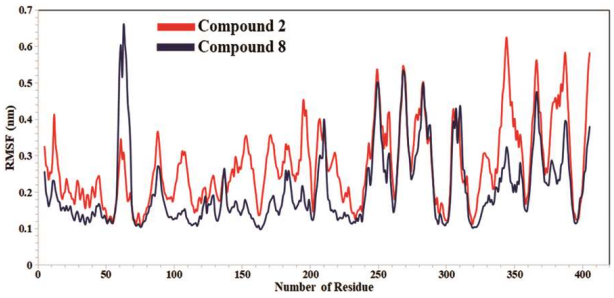

Fig. 7 — Root mean square fluctuation (RMSF) of the protein–ligand complex

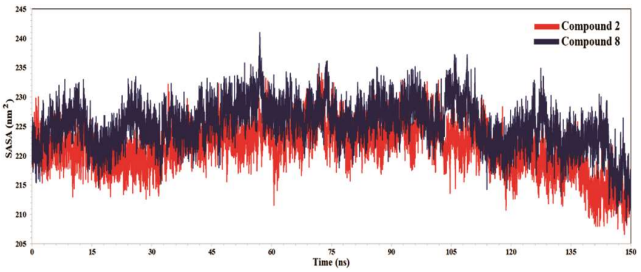

Fig. 8 — Total solvent accessible surface area (SASA) of the protein–ligand complex

complexed with compound **2** are consistently lower, fluctuating primarily between 215 and 228 nm². This trend suggested that the presence of compound **2** promoted a more compact conformation of the protein throughout the simulation. The reduced solvent exposure implies that compound **2** may induce tighter packing around the binding site or stabilize hydrophobic core interactions within the protein. Additionally, the relatively minor fluctuations in SASA over time reflect structural stability and suggest that the protein–ligand complex with compound **2** maintains a well-ordered conformation under dynamic conditions. These characteristics point to a potentially stronger and more stable binding interaction between compound **2** and the target protein. In contrast, the SASA values for the protein in complex with compound **8** are noticeably higher, ranging mostly between 220 and 235 nm², with

frequent fluctuations throughout the 150 ns simulation. This higher and more variable solvent exposure indicates a relatively less compact structure. The greater amplitude in SASA variation further suggests increased structural dynamics or local unfolding events in the presence of compound **8**. Overall, the SASA profile of compound **8** reflects a more solvent-exposed and less stable complex than that of compound **2**, which may be correlated with a reduced binding strength or fewer optimal interactions at the active site.

To assess the structural compactness and stability of compounds **2** and **8** during molecular dynamics simulations, the radius of gyration (Rog) was calculated and plotted as a function of simulation time, as shown in Fig. 9. Rog is a widely used metric that reflects the overall compactness of a molecular system by measuring the root mean square distance of atoms from their center of mass. A lower Rog value typically corresponds to a more compact and potentially more stable molecular conformation, whereas higher Rog values may indicate structural flexibility or expansion. The Rog profile of both compounds demonstrates a general downward trend over the course of the 150 ns simulation, suggesting progressive compaction and structural reorganization toward more stable conformations. Notably, compared with compound **8** (depicted in blue), compound **2** (represented in red) exhibited a more pronounced decrease in Rog over time. Initially, compound **2** displayed Rog values in the range of approximately 3.00–3.05 nm. Over the simulation duration, these values decreased steadily, stabilizing between 2.90 and 2.95 nm. This consistent decrease suggests that compound **2** underwent substantial conformational rearrangement, ultimately resulting in a more compact structure. In contrast, compound **8** began with slightly higher Rog values, ranging from 3.05 to 3.10 nm, and demonstrated a more gradual decline throughout the simulation. Toward the latter part of the trajectory, the Rog values for compound **8** plateaued at approximately 2.95 to 3.00 nm, indicating a less compact final structure relative to that of compound **2**. Furthermore, while compound **8** showed relatively stable Rog fluctuations throughout the simulation, compound **2** exhibited more pronounced fluctuations, particularly in the early stages, which may be indicative of conformational transitions or flexible regions adapting to a more energetically favorable state. Collectively, these findings suggest that, compared with compound **8**, compound **2** achieves greater structural compaction and dynamic stability. The more substantial reduction in Rog for compound **2** implies tighter packing and possibly a more rigid conformation, which could have implications for its biological activity, binding affinity, or resistance to denaturation. Moreover, the less pronounced compaction observed in compound **8** may reflect a greater degree of conformational flexibility, potentially influencing its functional interactions differently.

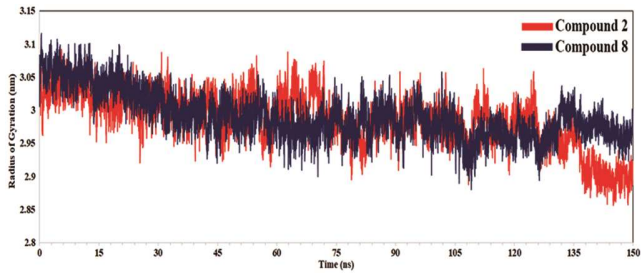

Fig. 9 — Radius of gyration (Rog) profiles of compounds **2** and **8** during MD simulation

ADMET Prediction

Absorption explains how a medicine enters the bloodstream after being administered[63]. Once in circulation, the drug is delivered to a variety of tissues and organs. The drug is then metabolized by the body *via* metabolism. Throughout this procedure, toxicity refers to a drug's potential adverse effects on the body. The primary goal of preclinical ADMET is to eliminate poor drug candidates in the early phases of drug development, allowing resources to be directed toward viable therapeutic candidates[64]. Pharmacokinetic parameters have been used to assess the absorption, metabolism, and toxicity of all methyl α-D-glucopyranoside derivatives, which are noncarcinogenic and have positive human intestine adsorption values. The acute oral toxicity of class three compounds makes them reasonably safe for oral consumption[65]. The movement of chemicals, ions, and cells between the brain and other parts of the body is constantly observed by the blood–brain barrier (BBB), which is a very restrictive barrier. The central nervous system is shielded by this barrier against toxins, infections, inflammation, trauma, and illness[66]. Compound **8** had the highest BBB values among the derivatives (+0.9314) (Table 7).

Prediction of Biological Activities

The antifungal, antipyretic, anti-inflammatory, anti-infective, antiviral and antidiabetic properties[67–69]

Table 7 — Selected pharmacokinetic parameters of methyl α-D-glucopyranoside and its derivatives

Entry	Absorption	Distribution		Metabolism	Toxicity		
	HIA	BBB	P-GpI	CYP450 2C9	hERG Inhibitor	Carcinogens	AOT
1	0.8373	0.6148	0.9393(NI)	0.9535 (NI)	0.9535(WI)	0.9654 (NC)	III
2	0.7708	0.7849	0.8180(NI)	0.9090(NI)	0.9806(WI)	0.9635(NC)	III
3	0.9474	0.8781	0.9114(I)	0.8220(NI)	0.9446(WI)	0.9012(NC)	III
4	0.9427	0.9183	0.9392(I)	0.8749(NI)	0.9039(WI)	0.9078(NC)	III
5	0.9427	0.9183	0.9392(I)	0.8749(NI)	0.9039(WI)	0.9078(NC)	III
6	0.9427	0.9183	0.9392(I)	0.8749(NI)	0.9039(WI)	0.9078(NC)	III
7	0.9427	0.9183	0.9392(I)	0.8749(NI)	0.9039(WI)	0.9078(NC)	III
8	0.8759	0.9314	0.6690(I)	0.7670(NI)	0.9437(WI)	0.8609(NC)	III

HIA = Human Intestinal Absorption, BBB = Blood–Brain Barrier, P-Gp*i*= P-Glycoprotein Inhibitor, hERG = Human Either A-Go-Go-Gene, ERB = Estrogen Receptor Binding, AOT = Acute Oral Toxicity, NI = Noninhibitor, *WI* = Weak Inhibitor, III = Category III includes compounds with LD50 greater than 500 mg/kg but less than 5000 mg/kg.

Table 8 — Prediction of the biological activities of methyl α-D-glucopyranoside and its derivatives *via* PASS

Entry	Anti-fungal	Anti-pyretic	Anti-inflammatory	Anti-infective	Anti-viral	Anti-diabetic
1	0.628	0.183	0.650	0.858	0.765	0.746
2	0.629	0.237	0.626	0.895	0.699	0.535
3	0.662	0.188	0.612	0.622	0.247	0.305
4	0.662	0.188	0.612	0.622	0.247	0.305
5	0.662	0.188	0.612	0.622	0.247	0.305
6	0.662	0.188	0.612	0.622	0.247	0.305
7	0.662	0.188	0.612	0.622	0.247	0.305
8	0.559	0.230	0.673	0.420	0.209	0.243

of methyl α-D-glucopyranoside and its derivatives were predicted *via* the PASS algorithm. PASS outcomes are revealed by Pa (probability for the active molecule) and Pi (probability for the inactive molecule[70]. With respect to potentialities, the Pa and Pi scores vary in the range of 0.00-1.00 and usually, Pa + Pi ≠1[71]. With the exception of derivative **8**, all the compounds outperformed methyl α-D-gluco-pyranoside in terms of antifungal properties. Derivatives **2** and **8** have significantly greater antipyretic properties, with values of 0.237 and 0.230, respectively. The anti-inflammatory property of derivative **8** (0.673) and the anti-infective property ofderivative **2** (0.895) are the greatest. The antiviral and antidiabetic properties of compounds **1** through **8** tended to decrease (Table 8).

Conclusion

This study analyzes the stability, reactivity, and pharmacokinetic properties of methyl α-D-glucopyranoside and its derivatives by computational chemistry. The free energy, enthalpy, and thermodynamic stability of methyl α-D-glucopyranoside and its derivatives were determined with thermodynamic analysis. This provides an understanding of their reactivity. Molecular orbital (FMO) investigations revealed that their HOMO–LUMO energy gaps, which aids in a better understanding of their reactivity. Molecular docking analysis revealed that the docked poses of the derivatives (**2**, **3** and **8**) with 3N40 had greater binding affinities and substantial nonbonding interactions than did the parent molecule. MD simulations reinforced the stability and strong binding interactions of complex **2** and **8**. The ADMET suggested that the modified derivatives had acute class three oral toxicity and were noncarcinogenic, with a positive BBB value. Our predictions revealed antifungal, antipyretic, anti-inflammatory, anti-infective, antiviral, and antidiabetic properties. This research aims to better understand the chemical, thermal, physicochemical, and pharmacokinetic aspects of methyl α-D-glucopyranoside derivatives.

Supplementary Information

Supplementary information is available in the website http://nopr.niscpr.res.in/handle/123456789/58776.

Conflict of Interest

The authors have no conflicts of interest to declare.

Acknowledgments

The authors are very thankful to the Ministry of Science and Technology (MoST) (Ref.: 39.00.0000. 006.99.026.24.65/SRG-246485), Bangladesh, for providing financial support for this work.

ORCID ID

Nazia Islam: https://orcid.org/0009-0009-7739-5366

Supriyo Saha: https://orcid.org/0000-0003-1365-4698

Sarkar M.A. Kawsar: https://orcid.org/0000-0001-7964-9117

References

1 Navarro D M D L, Abelilla J J& Stein H H, *J Anim Sci Biotech,* 10 (2019) 1.
2 Cummings J H & Stephen A M, *Eur J Clin Nutr*, 61 (2007) S5.
3 Pan L, Cai C, Liu C, Liu D, Li G, Linhardt R J & Yu G, *Curr Opin Biotech,* 69 (2021) 191.
4 Pifferi C, Fuentes R & Fernández-Tejada A, *Nat Rev Chem,* 5 (2021) 197.
5 Cipolla L & Peri F, *Mini-Rev Med Chem,*11 (2010) 39.
6 Kawsar S M A, Hosen M A, Bakri Y E, Ahmad S, Affi S T & Goumri-Said S, *Arab J Basic Appl Sci*, 29 (2022) 99.
7 Tiwari V K, *Chem Rec,* 21 (2021) 3029.
8 Kawsar S M A, Almalki F A, Hadda T B, Laaroussi H, Khan M A R, Hosen M A, Mahmud S, Aounti A, Maideen N M P, Heidarizadeh F &Soliman S S M, *Mol Simul,* 49 (2023) 60.
9 Asensio J L, Ardá A, Cañada F J & Jiménez-Barbero J, *Acc Chem Re,* 46 (2013) 946.
10 Lalhmangaihzuala S, Vanlaldinpuia K, Khiangte V, Laldinpuii Z, Liana T, Lalhriatpuia C &Pachuau Z, *Mol* Divers, 28 (2024) 4553.
11 Kawsar S M A, Ferdous J, Mostafa G &Manchur M A, *Chem Chem Tech,*8 (2014) 19–27.
12 Cao X, Du X, Jiao H, An Q, Chen R, Fang P, Wang J & Yu B, *Acta Pharm Sin B,* 12 (2022) 3783.
13 Kabir A K M S, Dutta P, Kawsar S M A, Bhuiyan M M R & Anwar M N, *Bull Pure Appl Sci,* 23C (2004)39.
14 Cao X, Du X, Jiao H, An Q, Chen R, Fang P, Wang J & Yu B, *Acta Pharm Sin B*, 12 (2022) 3783.
15 Kawsar S M A, Matsumoto R, Fujii Y, Matsuoka H, Masuda N, Chihiro I, YasumitsuH,Kanaly R A, Sugawara S, Hosono M, Nitta K, Ishizaki N, Dogasaki C, Hamako J, Matsui T & Ozeki Y, *Protein J*, 30 (2011) 509.
16 Matsumoto R, Fujii Y, Kawsar S M A, Kanaly R A, Yasumitsu H, Koide Y, Hasan I, Iwahara C, Ogawa Y, Im C H, Sugawara S, Hosono M, Nitta K, Hamako J, Matsui T & Ozeki Y, *Toxins*, 4 (2012) 323.
17 Fujii Y, Kawsar S M A, Matsumoto R, Yasumitsu H, Ishizaki N, Dogasaki C, Hosono M, Nitta K, Hamako J, Taei M & Ozeki Y, *Biochem Mol Biol,* 158 (2011) 30.
18 Fujii Y,Sarkar M A Kawsar, Matsumoto R, Yasumitsu H, Noriaki K &Ozeki Y, *J Biol Sci*,9 (2009) 319.
19 Kawsar S M A, Takeuchi T, Kasai K, Fujii Y, Matsumoto R, Yasumitsu H & Ozeki Y, *Comp Biochem Phys Part B Biochem Mol Bio*, 152 (2009) 382.
20 Kawsar S M A, Mostafa G, Huq E, Nahar N & Ozeki Y, *Int J Nat Eng Sci*, 3 (2009) 69.
21 Olennikov D N, Tankhaeva L M, Nikolaeva G G Tsyrenzhapov A V, Nikolaev S M & Chekhirova G V, *Chem Nat Comp,* 40 (2004) 1.
22 Lalhmangaihzuala S, Vanlaldinpuia K, Khiangte V, Laldinpuii Z, Liana T, Lalhriatpuia C &Pachuau Z, *Mol Divers,* 28 (2024) 4553.
23 Pan L, Cai C, Liu C, Liu D, Li G, Linhardt R J & Yu G, *Curr Opin Biotech*, 69 (2021) 191.
24 Kawsar S M A, Islam M, Jesmin S, Manchur M A, Hasan I & Rajia S,*Int J Biosci*, 12 (2018) 211.
25 Kabir A K, Kawsar S M A, Bhuiyan M M, Rahman M S & Banu B, *Chittagong Uni J Biol Sci*, 3 (2008) 53.
26 Khalil S M, *Z Naturforsch A*, 3 (2008) 42.
27 Kawsar S M A, Hosen M A, Fujii Y & Ozeki Y, *SDRP J Comput Chem Mol Mod***,** 4 (2020) 452.
28 Maowa J, Hosen M A, Alam A, Rana K M, Fujii Y, Ozeki Y & Kawsar S M A, *Phys Chem Res*, 9 (2021) 385.
29 Kawsar S M A, Hosen M A, Chowdhury T S, Rana K M, Fujii Y & Ozeki Y, *Rev Chim,* 72 (2021) 159.
30 Hosen M A, Alam A, Islam M, Fujii Y, Ozeki Y & Kawsar S M A, *Bulg Chem Comm,* 53 (2021) 327.
31 Amin M R, Yasmin F, Hosen M A, Dey S, Mahmud S, Saleh M A, Emran T Bin, Hasan I, Fujii Y, Yamada M, Ozeki Y & Kawsar S M A, *Molecules*, 26 (2021) 7016.
32 Karplus M & Petsko G A, *Nature,* 347 (1990) 631.
33 Shamsuddin T, Hosen M, Alam M, Emran T & Kawsar S M A, *Med-Sci Int Med J,* 10 (2021) 1373.
34 Saha S, Prinsa, Jakhmola, Mahato V, Srivastava A K, Dobhal A K & Kawsar S M A, *Philippine J Sci,* 152 (2023) 1953.
35 Islam M M, Hossain M A, Yamari I, Abchir O, Chtita S, Ali F & Kawsar S M A, *Chem Biodiver,* 21 (2024) e202400932.
36 Kawsar S M A, Hamida A A, Sheikh A U, Hossain M K, Shagir A C, Sanaullah A F M, Manchur M A, Imtiaj H, Ogawa Y, Fujii Y, Koide Y & Ozeki Y, *Int J Org Chem*, 5 (2015) 232.
37 Cabral O V, Téllez S C A, Giannerini T & Felcman J, *Spectrochim Acta A Mol BiomolSpect*, 61 (2005) 337.
38 Mustafa G, Shafiq I, Shaikh Q U A, Mustafa A, Zahid R, Rasool F, Asghar M A, Baby R, Alshehri S M & Haroon M, *ACS Omega*, 8 (2023) 22673.
39 Elokely K M & Doerksen R J, *J Chem Inf Model,* 53 (2013) 1934.
40 Schwede T,Kopp J,Guex N & Peitsch M C, *Nucleic Acids Res,* 31(2003) 3381.
41 Dallakyan S & Olson A J, *Methods Mol Biol*, 1263 (2015) 243.
42 Bjelkmar P, Larsson P, Cuendet M A, Hess B & Lindahl E, *J Chem Theory Comp,* 6(2010) 459.
43 Bugnon M, Goullieux M, Röhrig U F, Perez M A S, Daina A, Michielin O & Zoete V, *J Chem Inf Mod*, 63(2023) 6469.
44 Mark P & Nilsson L, *J Phys Chem A,* 105 (2001) 9954.
45 Yang H, Lou C, Sun L, Li J, Cai Y, Wang Z, Li W, Liu G & Tang Y, *Bioinformatics,*35 (2019) 1067.
46 Lipinski C A, Lombardo F, Dominy B W & Feeney P J, *Adv Drug Deliv Rev,* 23(1997) 3.
47 Gu Y, Yu Z, Wang Y, Chen L, Lou C, Yang C, Li W, Liu G & Tang Y, *Nucleic Acids Res,* 52 (2024) W432.
48 Munia N S, Alanazi M M, Bakri Y E, Alanazi A S, Mukhrish Y E, Hasan I & Kawsar S M A,*Medicina*, 59 (2023) 1107.
49 Habibyar A F, Sharma N & Khurana N, *Eur J Pharmacol*, 789 (2016) 385.
50 Filimonov D A, Lagunin A A, Gloriozova,T A, Rudik A V, Druzhilovskii D S, Pogodin P V &Poroikov V V, *Chem Heterocycl Comp,* 50 (2014) 444.
51 Kumar R, Kumar R, Anand A,Sharma N & Khurana N,*Asian J Pharm Clin Res,*11 (2018) 48.

52 Kollman P, *Chem Rev*, 93 (1993) 2395.
53 Lien E J, Guo Z R, Li R L & Su C T, *J Pharm Sci,* 71(1982) 641.
54 Parr R G & Zhou Z, *Acc Chem Res,* 26 (1993) 256.
55 Scrocco E & Tomasi J, *New Concepts,*42 (1973) 95. (https://doi.org/10.1007/3-540-06399-4_6)
56 Politzer P & Murray J S, *Rev Comput Chem*, 2 (1991) 273. (https://doi.org/10.1002/9780470125793.ch7).
57 Baiz C R, Błasiak B, Bredenbeck J, Cho M, Choi J.-H, Corcelli S. A, Dijkstra A G, Feng C J, Garrett-Roe S, Ge N.-H, Hanson-Heine M. W. D, Hirst J D, Jansen T L C, Kwac K, Kubarych K J, Londergan C H, Maekawa H, Reppert M, Saito S, Roy S, Skinner J L, Stock G, Straub J E, Thielges M C,Tominaga K, Tokmakoff A, Torii H, Wang L, Webb L J & Zanni M T, *Chem Rev,* 120 (2020) 7152.
58 Akter N, Saha S, Hossain M A, Uddin K M, Bhat A R, Ahmed S & Kawsar S M A, *Chem Phys Impact*, 9 (2024) 100700.
59 Andersson M P &Uvdal P, *J Phys Chem A,* 109 (2005) 2937.
60 Brown J Q, Vishwanath K, Palmer G M & Ramanujam N, *Curr Opin Biotech,* 20 (2009) 119.
61 Singh S, Baker Q B & Singh D B, *J Bioinform,* (2022) 291. (https://doi.org/10.1016/B978-0-323-89775-4.00014-6).
62 Arzine A, Hadni H, Boujdi K, Chebbac K, Barghady N, Rhazi Y, Chalkha M, Nakkabi A, Chkirate K, Mague J T, Kawsar S M A, Al Houari G, M Alanazi M & El Yazidi M, *Molecules,* 29 (2024) 3366.
63 Lotfi B, Mebarka O, Alhatlani B Y, Abdallah E M & Kawsar S M A, *Molecules,* 28 (2023) 6678.
64 Hodgson J, *Nat Biotechnol,* 19 (2001) 722.
65 Walum E, *Environ Health Perspect,* 106(1998) 497.
66 Daneman R, *Ann Neurol,* 72 (2012) 648.
67 Devi S R, Jesmin S, Rahman M, Manchur M A, Fujii Y, Ozeki Y & Kawsar S M A, *Acta Pharm,* 57 (2019) 47.
68 Arifuzzaman, Islam M M, Rahman M M, Rahman M A &Kawsar S M A, *ACTA Pharm Sci,* 56 (2018) 7.
69 Kabir AK M S, Kawsar S M A, Bhuiyan MM R, Rahman M S & Chowdhury M E, *Pak J Sci Ind Res,* 52 (2009) 138.
70 Munia N S, Hosen M A, Azzam K M A, Al-Ghorbani M, Baashen M, Hossain M K, Ali F, Mahmud S, Shimu M S S, Almalki F A, Hadda T B, Laaroussi H, Naimi S & Kawsar S M A, *NucleosNucleot Nucleic Acids*, 41(2022) 1036.
71 Lagunin A, Stepanchikova A, Filimonov D & Poroikov V, *J Bioinform,* 16(2000) 747.